Explanation and modelling of angle-dependent scattering in polymer optical fibres

Lukasz Jankowski
Federal Institute for Materials Research and Testing (BAM)
Unter den Eichen 87, D-12200 Berlin, Germany
lukasz.jankowski@bam.de

13th Int. Conf. on Plastic Optical Fibres
27-30 September 2004, Nuremberg, Germany, pp. 195-202

Summary
Simulations and measurements of optical fibres suggest that the higher the illumination angle, the less is the scattering intensity. However, the geometric optic and raytracing analysis clearly give the opposite relation. Therefore the wave analysis is applied to scattering. As a result a ready-to-use formula for the scattering intensity in dependence on the illumination angle is obtained. Four numerical examples are reported, their results confirm the expected decrease in scattering with increasing illumination angle.

1. Introduction

Besides attenuation, important basic characteristics of optical fibres are their scattering properties, induced by non-uniformities of fibre's refractive index and geometry. Scattering is present in all approaches to fibre modelling:

- Within the wave optics framework it is represented by the power transfer between propagating modes [4,5,7-11].
- Raytracing models of the geometric optics include scattering in the form of periodic redirections of traced rays on its way through the modelled fibre [2,6].
- The angular dispersion model first proposed by Gloge [1] uses local mixing intensity coefficient to model continuous power transfer between neighbouring directions of propagation.

The Gloge's dispersion model [1] as well as some of the raytracing models [2] assume constant scattering intensity, independent of propagating angle. Others [3,6] suggest that at least in some fibres scattering is angle-dependent (it should be more intense for lower order modes than for higher order modes) and propose purely phenomenological curves of scattering intensity distribution.

The angle-dependence of scattering also seems to be confirmed by far-field profile (FFP) measurements (Fig. 1, 2). Fig. 1 compares three FFPs of 10 m POF sample, laser-illuminated at 6°, 15° and 24° and normalised to 100 % height. Decreasing widths of the graph peaks suggest that the scattering intensity decreases with illumination angle. Fig. 2 compares normalised FFPs of 10 m samples of POF from two manufacturers, laser-illuminated at 6° and 24°. The ESKA fibre (solid line) at high illumination angle (24°) clearly shows much less scattering than the LUMINOUS fibre (dashed line). At low illumination angle (6°) the relation is opposite, the ESKA fibre shows slightly more scattering than the other fibre. The measurements suggest different, thus not constant, angle-dependence of scattering intensity in both fibres.

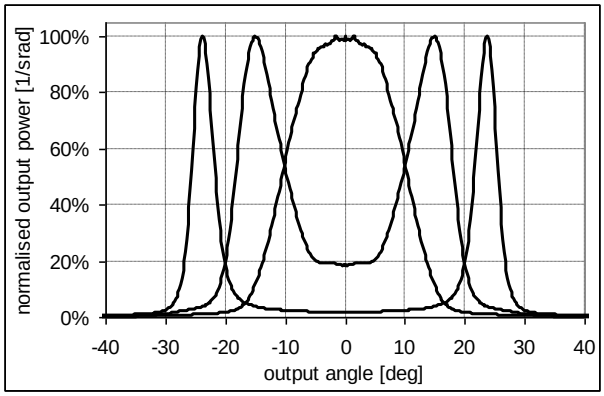

Fig. 1 Normalised FFPs of 10 m ESKA CK-40 POF, illumination angles 6°, 15° and 24°.

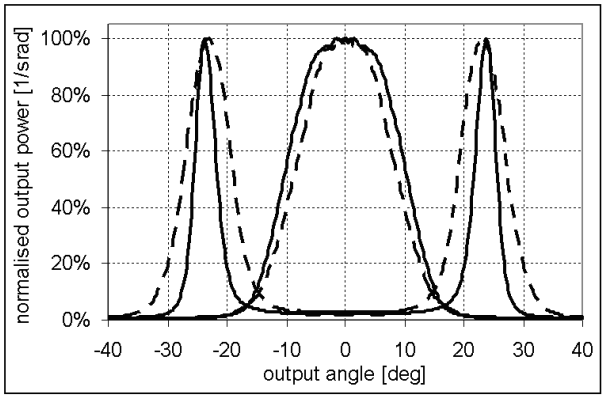

Fig. 2 Normalised FFPs of 10 m ESKA CK-40 (solid line) and LUMINOUS TB-1000 (dashed line) POF, illumination angles 6° (left) and 24° (right).

The decreasing scattering intensity with increasing illumination angle, although confirmed by measurements and simulations [see e.g. 6], seems to be hard to explain using geometric optics only, as this approach implicates generally the opposite relation. Rays launched at higher angles cover longer path within the fibre and undergo more reflections on the core-clad interface, thus (under the assumption of uniform distribution of perturbations within the core) they should be expected to get more scattered than the rays launched at lower angles. The same mechanism (longer path, more reflections) causes the increase in attenuation for higher illumination angles.

Therefore explaining the contrary actual scattering dependence, if possible at all, would require elaborate and unrealistic shapes of refractive index perturbations. Thus the wave analysis is used for explanation. We will focus mostly on practical issues, restricting the mathematical details as far as possible.

2. Fibre modes

For describing fibre modes we will use the scalar wave equation and follow the analysis of Alexandrov and Ciraolo [12]. The scalar wave equation is a simplified version of the vector wave equation, valid in the case of small variations of refractive index [1]. It has the form:

$$\Delta u + n^2 k^2 u = 0\,, \tag{1}$$

where u denotes one of the transversal coordinates of the electric field, k is the free-space wavenumber and n is the (unperturbed) refractive index of the fibre, defined by:

$$n(r) = \begin{cases} n_0\,, & r \in [0, R] \quad \text{(core)}, \\ n_1 < n_0\,, & r \in (R, \infty), \quad \text{(clad)}, \end{cases} \tag{2}$$

where R is the radius of the core. Solving Eq. (1) by separation of variables in the cylindrical coordinate system (r,φ,z) and taking into account the obvious requirements (a) $\partial u/\partial r$ exists and is continuous (b) u is bounded, two sets of solutions are obtained: a discrete (and maybe empty) set of *guided modes* and a continuous set of *radiating modes*. Modes of both kinds have the following form:

$$n(r, \varphi, z) = \exp(ik\beta\, z + im\varphi) \cdot j_m\left(r, \beta^2\right), \tag{3}$$

where β is the relative wavenumber of the mode ($k\beta$ is the mode propagation constant), $m \in \mathbf{Z}$ due to the conservation condition and j_m: $\mathbf{R} \to \mathbf{R}$ is the radial component of the propagating mode. For notational clarity the following symbols will by used:

$$\begin{aligned} \tau &:= \beta^2, & w_0 &:= k\sqrt{\left|n_0^2 - \tau\right|}, \\ V &:= wR, & w_1 &:= k\sqrt{\left|n_1^2 - \tau\right|} < w_0, \end{aligned} \tag{4}$$

where V is a mode-independent waveguide parameter (often called waveguide's *normalised frequency*). For a typical POF $V \approx 4000$, which corresponds to more than 10^6 guided modes. A respective *guided mode* exists for given $m \in \mathbf{Z}$ and $\tau \in \left(n_1^2, n_0^2\right)$ if and only if the following equation holds

$$w_0 R \frac{J_{m+1}(w_0 R)}{J_m(w_0 R)} = w_1 R \frac{K_{m+1}(w_1 R)}{K_m(w_1 R)}, \tag{5}$$

where J is the real Bessel functions of the first kind and K is the real modified Bessel function of the second kind. If Eq. (5) holds, then the radial component j_m of the respective guided mode decays exponentially in the clad with r and takes the form:

$$j_m(r,\tau) = \begin{cases} J_m(w_0 r), & r \in [0, R] \\ \dfrac{J_m(w_0 R)}{K_m(w_0 R)} K_m(w_1 r), & r \in (R, \infty). \end{cases} \tag{6}$$

A respective *radiation mode* exists for each $m \in \mathbf{Z}$, $\tau \in \left(-\infty, n_1^2\right)$, it extends oscillating into the clad and its radial component j_m takes the form:

$$j_m(r,\tau) = \begin{cases} J_m(w_0 r), & r \in [0, R] \\ a_m(\tau) \cdot J_m(w_1 r) + b_m(\tau) \cdot Y_m(w_1 r), & r \in (R, \infty), \end{cases} \tag{7}$$

where Y denotes the real Bessel function of the second kind and

$$\begin{aligned} a_m(\tau) &= \frac{1}{2} R\pi \left[w_0 J_{m+1}(w_0 R) Y_m(w_1 R) - w_1 J_m(w_0 R) Y_{m+1}(w_1 R)\right], \\ b_m(\tau) &= \frac{1}{2} R\pi \left[w_1 J_{m+1}(w_1 R) J_m(w_0 R) - w_0 J_m(w_1 R) J_{m+1}(w_0 R)\right]. \end{aligned} \tag{8}$$

In principle there can exist also another type of guided modes that decay in the clad with $r^{-|m|}$, but such modes will not occur in the numerical examples of this paper and thus are skipped here. Therefore, the formulae Eq. (3), Eq. (6) and Eq. (7) describe the modal fields of all guided modes present in the fibres analysed in this paper.

3. Illumination, modal fields and output FFP

Alexandrov and Ciraolo have proved in [12] that each finite-power field $u(r,\varphi,z)$ propagating in a cylindrical fibre can be uniquely represented as a superposition of guided and radiation modes in the form

$$u(r,\varphi,z) = \frac{1}{\pi} \sum_{m \in \mathbf{Z}} \exp(im\varphi) \cdot \int_{-\infty}^{+\infty} j_m(r,\tau) \cdot G_m(\tau, z)\, d\chi_m(\tau), \tag{9}$$

where

$$G_m(\tau, z) := \int_0^{\infty} r \cdot j_m(r,\tau) \cdot u_m(r,z)\, dr \tag{10}$$

with $u_m(r,z)$ being the Fourier coefficients of $u(r,\varphi,z)$:

$$u_m(r,z) := \frac{1}{2\pi} \int_0^{2\pi} e^{-im\varphi} \cdot u(r,\varphi,z)\, d\varphi \tag{11}$$

The function $\chi_m(\tau)$ in Eq. (9) is for $\tau \in \left[n_1^2, \infty\right)$ constant between the discontinuity points $\left\{\tau_k^m \,\middle|\, k = 1, \ldots, P_m\right\}$ being the solutions to Eq. (5), in which it has jumps

$$r_k^m := \pi\left(\int_0^\infty r \cdot j_m^2\left(r, \tau_k^m\right) dr\right)^{-1}. \tag{12}$$

For $\tau \in \left(-\infty, n_1^2\right)$ the function $d\chi_m(\tau)$ is defined as:

$$\chi_m(\tau) := \frac{1}{2} \frac{k^2 \pi}{a_m^2(\tau) + b_m^2(\tau)}. \tag{13}$$

Finally, the Parseval identity holds, too [12]:

$$\int_0^\infty r \cdot \int_0^{2\pi} |u(r, \varphi, z)|^2 \, d\varphi \, dr = 2 \sum_{m \in \mathbf{Z}} \int_{-\infty}^{+\infty} |G_m(\tau, z)|^2 \, d\chi_m(\tau). \tag{14}$$

The representation Eq. (9) can be used to find the excitations of modes in the fibre with uniformly laser-lighted input face. Let only the core area be lighted on the fibre input face by a plane wave with the direction of propagation contained in the x-z surface, uniformly polarized in y-axis direction and with incident angle α with the fibre axis. Assuming that the fields at the input face are approximately those at the boundary between two semi-infinite media of refractive indices 1 (air) and n_0 (core), the field u at the input face can be computed from standard formulae for plane-wave refraction at a dielectric interface (Fig. 3).

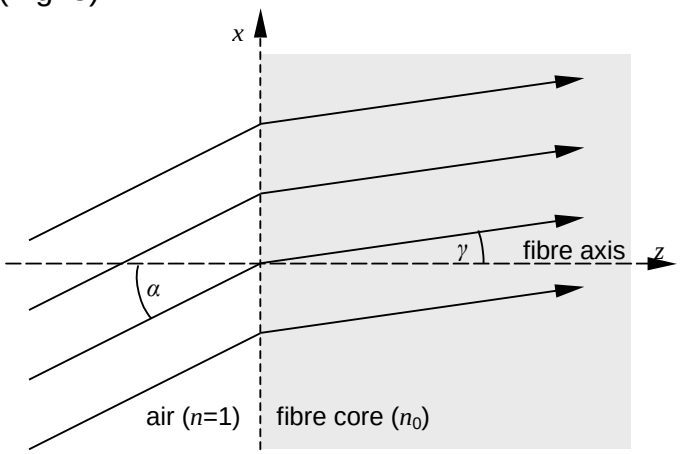

Fig. 3 Refraction of a beam at the input face of an optical fibre.

Neglecting the Fresnel refraction coefficients, normalising to keep constant the total power illuminating the fibre core and using the expansion to series of Bessel functions, the following expression for the field u in the core at $z = 0$ can be obtained:

$$u(r, \varphi, 0) = \mathbf{1}_{core}\left[e^{ikn_0 x \sin\gamma}\right] = \mathbf{1}_{core}\left[e^{ikx\sin\alpha}\right] = \mathbf{1}_{core}\left[e^{ikr\cos\varphi\sin\alpha}\right] = \mathbf{1}_{r\in[0,R]}\left[\sum_{m\in Z} i^m e^{im\varphi} J_m(kr\sin\alpha)\right]. \tag{15}$$

Eq. (10) and Eq. (11) yield

$$(G_0)_m(\alpha;\tau) = \frac{i^m R}{w_0^2 - k^2 \sin^2\alpha}\left[k\sin\alpha \cdot J_m(w_0 R) \cdot J_{m-1}(kR\sin\alpha) - w_0 J_m(kR\sin\alpha) \cdot J_{m-1}(w_0 R)\right] \tag{16}$$

and Eq. (14) allows writing the formula for the angle-dependent power launched into a guided mode:

$$p_m^{(0)}\left(\alpha; m, \tau_k^m\right) = 2r_k^m \left|(G_0)_m\left(\alpha; \tau_k^m\right)\right|^2. \tag{17}$$

Summing Eq. (17) over all guided modes gives the angle-dependent total power launched into guided modes of a fibre. Fig. 4 shows the part of the power launched into the guided modes (normalised sum over Eq. (17)) of two sample fibres in dependence on the illumination angle.

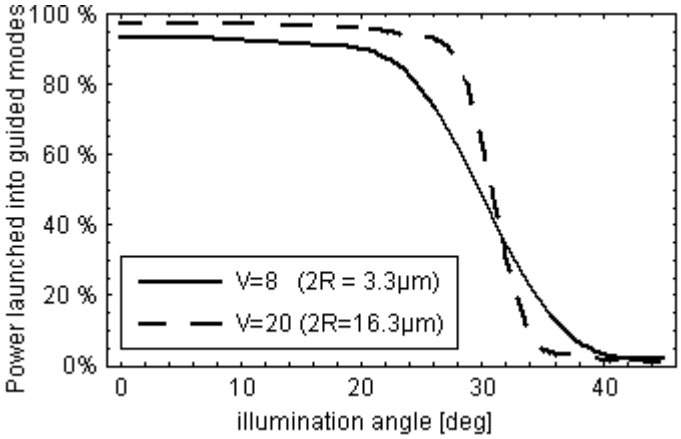

Fig. 4 Relative power launched the guided modes in dependence on illumination angle for $V = 8$ ($2R = 3.3\ \mu$m) and $V = 20$ ($2R = 16.3\ \mu$m) waveguides.

Fig. 4 clearly suggests that with increasing fibre radius R (or normalised frequency V) almost all power incident within the acceptance angle enters guided modes and so the limiting graph is step-like, see [5, chapter 20].

4. Non-uniformities of the refractive index and induced scattering

In an ideal non-absorbing fibre the refractive index profile as well as the power distribution between modes are steady along the waveguide's length. However, slight refractive index perturbations are inevitable in a real waveguide and give rise to the continuous power flow between modes, referred to as the scattering, mode mixing or coupling. We will follow the approach of Magnanini and Santosa [4] and expand their two-dimensional analysis of scattering in a slab waveguide to the three-dimensional case of an optical fibre.

The refractive index n of an ideal fibre in Eq. (2) depends only on the radius r. The perturbed fibre has a refractive index $n_p(r,\varphi,z)$, defined by the perturbation function $d(r,\varphi,z)$ with a bounded support:

$$\begin{aligned} n_p^2(r,\varphi,z) &:= n^2(r) + d(r,\varphi,z), \\ \text{supp}\ d(r,\varphi,z) &= \Omega = [0,R_0)\times[0,2\pi)\times(0,z_0). \end{aligned} \tag{18}$$

Decomposing the total field u in Eq. (1) to the sum of the incident and scattered fields and substituting n_p from Eq. (20) lead to a variant of the Helmholtz equation:

$$\Delta u_{scat} + n^2 k^2 u_{scat} = -uk^2 d\,. \tag{19}$$

The scattered field has to satisfy some form of radiation conditions guaranteeing its uniqueness. As their exact form is not known even in the two-dimensional case [4], we will use, as in [4, 12], the solution that makes physical sense, based on the requirement that the waves are bounded and outgoing in the sense specified in [12]. The solution to Eq. (19) (assumed to be unique) can be written in the form

$$u_{scat} = Tu\,, \tag{20}$$

with the operator T defined as

$$Tu(r,\varphi,z) := -k^2 \int_{\Omega} d(\rho,\eta,\xi)u(\rho,\eta,\xi)g(r,\varphi,z;\rho,\eta,\xi)dV(\rho,\eta,\xi), \tag{21}$$

and $g(r,\varphi,z;\rho,\eta,\xi)$ being the Green's function of a homogenous fibre, found in [12] to be:

$$g(r,\varphi,z;\rho,\eta,\xi) = -\frac{i}{4\pi^2 k}\sum_{m\in Z} e^{im(\varphi-\eta)} \int_{-\infty}^{+\infty} \frac{1}{\beta} e^{i|z-\xi|k\beta} \cdot j_m(r,\tau)\cdot j_m(\rho,\tau)d\chi_m(\tau)\,. \tag{22}$$

Eq. (19) and Eq. (20) are satisfied by the von Neumann series [4, 13]:

$$u_{scat}(r,\varphi,z)=\sum_{l=1}^{\infty}u_l(r,\varphi,z), \qquad \begin{aligned} u_0(r,\varphi,z) &:= u_{inc}(r,\varphi,z), \\ u_{l+1}(r,\varphi,z) &:= Tu_l(r,\varphi,z). \end{aligned} \tag{23}$$

As Magnanini and Santosa did in [4] in the two-dimensional case, we will use in the further computations the Born approximation, i.e. only the first term of series Eq. (23):

$$u_{scat}(r,\varphi,z)\approx Tu_{inc}(r,\varphi,z)=-k^2\int_{\Omega}d(\rho,\eta,\xi)u_{inc}(\rho,\eta,\xi)g(r,\varphi,z;\rho,\eta,\xi)dV(\rho,\eta,\xi), \tag{24}$$

Eq. (10), Eq. (11) and the orthogonality of $\{\exp(im\varphi)|m\in\mathbf{Z}\}$ allow obtaining the scattered field and excitations of guided modes *after* the perturbation, i.e. for $z \geq z_0$:

$$(G_{scat})_m(z,\tau)=\frac{ik}{4\pi\beta}e^{ik\beta z}\int_{\Omega}d(\rho,\eta,\xi)\cdot u_{inc}(\rho,\eta,\xi)\cdot e^{-im\eta-ik\beta\xi}\cdot j_m(\rho,\tau)dV(\rho,\eta,\xi). \tag{25}$$

If assumed that the incident field consists of exactly one guided mode, i.e. that

$$u_{inc}(r,\varphi,z)=\exp(ik\beta_0 z+im_0\varphi)\cdot j_m(r,\tau_0), \tag{26}$$

where $\tau_0=\beta_0^2$, then Eq. (25) can be rewritten for $z \geq z_0$ in the following form:

$$(G_{scat})_m(z,\tau)=\frac{ik}{4\pi\beta}e^{ik\beta z}\int_{\Omega}d(\rho,\eta,\xi)\cdot e^{i(m_0-m)\eta}e^{ik(\beta_0-\beta)\xi}\cdot j_{m_0}(\rho,\tau_0)\cdot j_m(\rho,\tau)dV(\rho,\eta,\xi). \tag{27}$$

Eq. (27), given the form of refractive index perturbations $d(r,\varphi,z)$, together with the Parseval identity Eq. (14) and under the Born approximation Eq. (24) may be used to compute the power transfer coefficients between modes caused by the refractive index perturbations. If Eq. (26) represents the incident field, then the **r**elative **s**cattered **p**ower in LP_{mk} mode *after* the perturbation equals

$$rsp(m_0,k_0;m,k):=\frac{r_k^m r_{k_0}^{m_0}}{\pi^2}\left|(G_{scat})_m\left(z_0,\tau_k^m\right)\right|^2. \tag{28}$$

Using Eq. (17) for the excitation of guided modes the **t**otal **s**cattered **p**ower in dependence on the illumination angle α can be written down as

$$tsp(\alpha):=\sum_{m_0\in Z}\sum_{k_0=0}^{P_m}p_{m_0}^{(0)}\left(\alpha;m_0,\tau_{k_0}^{m_0}\right)\sum_{m\in Z}\sum_{k=0}^{P_m}rsp(m_0,k_0;m,k). \tag{29}$$

Eq. (29) is used in the next part to investigate on numerical examples the angle-dependence of scattering.

5. Numerical examples

Given the refractive index perturbation function $d(r,\varphi,z)$, formulae Eq. (27) to Eq. (29) can be used to investigate the angular dependence the total scattered power. For numerical computations a finite sum of simple single perturbations can be used:

$$d(\rho,\eta,\xi)=\sum_{l=1}^{L}A_l\exp\left[-\frac{\delta^2(\rho,\eta,\xi;\rho_l,\eta_l,\xi_l)}{S_l^2}\right], \tag{30}$$

where the point (ρ_l,η_l,ξ_l) is the centre of a single perturbation, A_l is its amplitude and S_l defines its e^{-1}-radius. The best candidate for the distance function δ would be the Euclidean metric

$$\begin{aligned} \delta^2(\rho_0,\eta_0,\xi_0;\rho_1,\eta_1,\xi_1) &= (\xi_0-\xi_1)^2+(\rho_0\cos\eta_0-\rho_1\cos\eta_1)^2+(\rho_0\sin\eta_0-\rho_1\sin\eta_1)^2= \\ &= (\xi_0-\xi_1)^2+\rho_0^2+\rho_1^2-2\rho_0\rho_1\cos(\eta_0-\eta_1), \end{aligned} \tag{31}$$

but this form would make the integral Eq. (27) not symbolically integrable and considerably increase its computation time. So the following function was used instead, a modified version of Eq. (31):

$$\begin{aligned} \delta^2(\rho_0,\eta_0,\xi_0;\rho_1,\eta_1,\xi_1) &= (\xi_0-\xi_1)^2+\rho_0^2+\rho_1^2-2\rho_0\rho_1\left[1-2|\eta_0-\eta_1|/\pi\right]= \\ &= (\xi_0-\xi_1)^2+(\rho_0-\rho_1)^2+4\rho_0\rho_1|\eta_0-\eta_1|/\pi, \end{aligned} \tag{32}$$

where $\cos(\eta_0\text{-}\eta_1)$ was approximated for $(\eta_0\text{-}\eta_1)\in(-\pi,\pi]$ with the saw function $1\text{-}2|\eta_0\text{-}\eta_1|/\pi$, what equals the effect of keeping the Euclidean metric Eq. (31) but modifying slightly the perturbation function Eq. (30). Substituting Eq(30) and Eq. (32) into Eq. (27) and changing the order of integration over Ω yield:

$$\begin{aligned}(G_{scat})_m(z,\tau) = \frac{ik}{4\beta\pi} e^{ik\beta z} \sum_{l=1}^{L} A_l \int_0^{z_0} \exp\left[ik(\beta_0-\beta)\xi - \left(\frac{\xi-\xi_l}{S_l}\right)^2 \right] d\xi \cdot \\ \cdot \int_0^{R_0} \exp\left[-\left(\frac{\rho-\rho_l}{S_l}\right)^2 \right] \cdot \rho \cdot j_m(\rho,\tau) j_{m_0}(\rho,\tau_0) \cdot \int_{\eta_l-\pi}^{\eta_l+\pi} \exp\left[i(m_0-m)\eta - \frac{4}{\pi S_l^2}\rho\rho_l|\eta-\eta_l| \right] d\eta\, d\rho\end{aligned} \quad (33)$$

First and third integrals of Eq. (33) can be computed analytically:

$$\begin{aligned}(G_{scat})_m(z,\tau) = \frac{k\sqrt{\pi}}{i\beta} e^{ik\beta z} \sum_{l=1}^{L} \rho_l A_l S_l \exp\left[-\frac{1}{4}k^2 S_l^2(\beta_0-\beta)^2 + i(\beta_0-\beta)k\xi_l \right] \cdot \\ \cdot \Phi\left[\frac{\xi_l - z_0}{S_l} + \frac{1}{2}ikS_l(\beta_0-\beta), \frac{\xi_l}{S_l} + \frac{1}{2}ikS_l(\beta_0-\beta) \right] \cdot \exp\left[i(m_0-m)\eta_l \right] \cdot \\ \cdot \int_0^{R_0} \rho^2 \cdot j_m(\rho,\tau) j_{m_0}(\rho,\tau_0) \cdot \exp\left[-\left(\frac{\rho-\rho_l}{S_l}\right)^2 \right] \cdot \frac{1-\exp\left[-\frac{4\rho\rho_l}{S_l^2} - i\pi(m+m_0) \right]}{\left[\pi S_l(m_0-m)\right]^2 + \left[\frac{4\rho\rho_l}{S_l}\right]^2} d\rho,\end{aligned} \quad (34)$$

where $\Phi(a,b)$ is the error function:

$$\Phi(a,b) = \frac{2}{\sqrt{\pi}} \int_a^b e^{-t^2} dt. \quad (35)$$

The remaining one-dimensional integral over $[0,R_0)$ has to be computed numerically. Using Eq. (34) it is easy to compute numerically the total scattered power $tsp(\alpha)$ Eq. (29) for a given illumination angle α. As it turned out to be highly dependent on the location and size of the waveguide perturbations, the results had to be averaged for several randomly drawn perturbations. The following perturbation properties were assumed:

- Only the fibre's core is perturbed, so $R_0=R$ in Eq. (34).
- The perturbation centre (ρ_l,η_l,ξ_l) is uniformly distributed within the core.
- The perturbation amplitude $A_l \sim N(0,A)$ (was modelled with a random variable of normal distribution with the mean 0 and the standard deviation A). Eq. (34) depends linearly on the perturbation amplitude, thus its exact value does not matter, all numerical computations were done with the constant value $A = 0.01$.
- The perturbation size $S_l \sim S\chi_1$ (was modelled with a random variable of chi-square distribution with one degree of freedom and the mean S).
- The perturbed fragment of the fibre has the length $z_0 = 10R$.

The computations were done

- a single perturbation (L=1 in Eq. (30)),
- two perturbation sizes (S=0.05R and S=0.25R)

and were repeated for two sample fibres (V=8, which corresponds to 17 guided modes and the diameter $2R$=3.3 μm, and V=20 (105 guided modes, $2R$ = 16.3 μm)). In each case 800 (for the V=8 fibre) or 400 (for the V=20 fibre) computations were made and averaged to obtain all scattering coefficients $rsp(m_0,k_0;m,k)$ (see Eq. (28)).

Fig. 5 plots the normalised total scattered power $tsp(\alpha)/tsp(0)$ (Eq. (29)) in dependence on the illumination angle α for both investigated fibres and perturbation sizes. On all four examples the strong decrease of total scattered power with increasing illumination angle is confirmed.

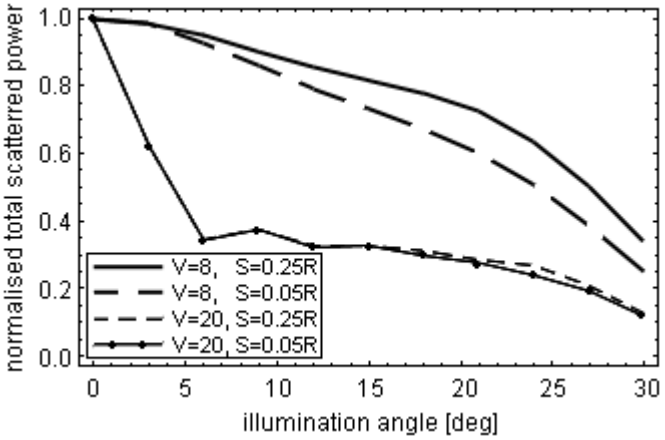

Fig. 5 Normalised total scattered power in dependence on the illumination angle for two sample waveguides and two sample perturbation sizes.

6. Conclusions

In this paper the wave analysis of Magnanini and Santosa [4] of scattering mechanisms in 2D slab waveguides was expanded to real cylindrical 3D fibres using the approach of Alexandrov and Ciraolo [12]. As a result the direct formula Eq. (29) for the total scattered power in dependence on the illumination angle was obtained and used in four numerical examples. Their results clearly confirm that the higher illumination angle, the less is the scattering intensity, in accordance with measurements and simulations but contrary to the explanation offered by the raytracing model.

Acknowledgements

The author would like to thank Prof. Klein and Prof. Holschneider from the Potsdam University and all the colleagues at BAM for numerous fruitful discussions and support.

References

[1] D. Gloge, *Optical power flow in multimode fibres*, Bell Syst. Tech. J. 51, 1972, pp. 1767-1783.

[2] L. Jankowski, A. Appajaiah, C.-A. Bunge, J. Zubia, *Modelling of Light Propagation Through Aged and Non-Aged POFs*, Proceedings of the 12th POF-IC, Seattle 2003.

[3] L. Jeunhomme, M. Fraise, J. P. Pocholle, *Propagation model for long step-index optical fibers*, Applied Optics 15(12), 1976, pp. 3040-3046.

[4] R. Magnanini, F. Santosa, *Scattering in a 2-D optical waveguide*, in: *Analytical and Computational Methods in Scattering and Applied Mathematics*, ed. F. Santosa, I. Stakgold, CRC Press, London 1999.

[5] A. Snyder, J. Love, *Optical Waveguide Theory*, Chapman and Hall, London New York, 1983.

[6] J. Zubia, H. Poisel, C.-A. Bunge, G. Aldabaldetreku, J. Arrue, *POF modelling*, Proceedings of the 11th POF-IC, Tokyo 2002, pp. 221-224.

[7] D. Marcuse, *Coupled Mode Theory of Round Optical Fibres*, Bell Syst. Tech. J., Vol. 52, 1973, pp. 817-842.

[8] I. White, A. Snyder, *Radiation from dielectric optical waveguides: a comparison of techniques*, Appl. Optics, Vol. 16(6), 1977, pp. 1470-1472.

[9] A. Snyder, *Excitation and Scattering of Modes on a Dielectric or Optical Fiber*, IEEE Trans. Microwaves Theory Techn., Vol. 17(12), 1969, pp. 1138-1144.

[10] A. Snyder, *Radiation Losses Due to Variations of Radius on Dielectric or Optical Fibres*, IEEE Trans. Microwaves Theory Techn., Vol. 18(9), 1970, pp. 608-615.

[11] E. Rawson, *Analysis of Scattering from Fiber Waveguides with Irregular Core Surface*, Appl. Optics, Vol. 13(10), 1974, pp. 2370-2377.

[12] O. Alexandrov, G. Ciraolo, *Wave propagation in a 3-D optical waveguide*, Mathematical Models and Methods in Applied Sciences (M3AS), Vol. 14(6), 2004, pp. 819-852.

[13] A. D. Polyanin, A. V. Manzhirov, *Handbuch der Integralgleichungen*, Spektrum Akademischer Verlag; Heidelberg, Berlin 1999.